



Unique design of superior metal-organic framework for removal of toxic chemicals in humid environment *via* direct functionalization of the metal nodes



Ga-Young Cha^{a,b,1}, Hoje Chun^{c,1}, Do-Young Hong^{a,b,1}, Jaegyeom Kim^d, Kyung-Ho Cho^a, U-Hwang Lee^{a,b}, Jong-San Chang^{a,e}, Sam Gon Ryu^{f,**}, Hae Wan Lee^f, Seung-Joo Kim^{d,**}, Byungchan Han^{c,**}, Young Kyu Hwang^{a,b,*}

^a Research Center for Nanocatalysts, Korea Research Institute of Chemical Technology (KRICT), Jang-dong, Yuseong, Daejeon 34114, Republic of Korea

^b Department of Advanced Materials and Chemical Engineering, University of Science and Technology (UST), Gajeong-dong, Yuseong, Daejeon 34113, Republic of Korea

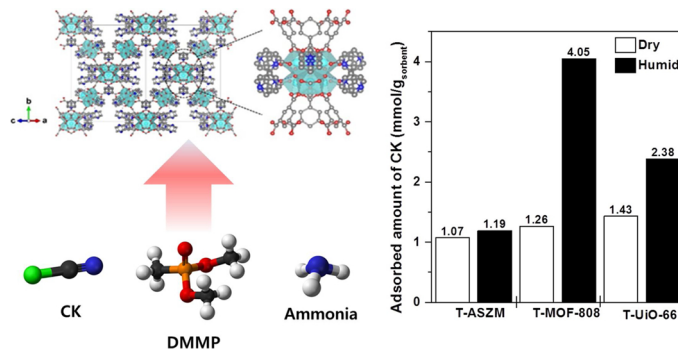
^c Department of Chemical and Biomolecular Engineering, Yonsei University, Sinchon-dong, Seodaemun, Seoul 03722, Republic of Korea

^d Department of Energy Systems Research, Department of Chemistry, Ajou University, Woncheon-dong, Yeongtong, Suwon 16499, Republic of Korea

^e Department of Chemistry, Sungkyunkwan University, Cheoncheon-dong, Jangan, Suwon 16419, Republic of Korea

^f Agency for Defense Development, Sunam-dong, Yuseong, Daejeon 34186, Republic of Korea

GRAPHICAL ABSTRACT



ARTICLE INFO

Editor: Xiaohong Guan

Keywords:

MOF

Surface functionalization

CWA

Toxic chemical

DFT

ABSTRACT

Unique chemical and thermal stabilities of a zirconium-based metal-organic framework (MOF) and its functionalized analogues play a key role to efficiently remove chemical warfare agents (ex., cyanogen chloride, CNCl) and simulant (dimethyl methylphosphonate, DMMP) as well as industrial toxic gas, ammonia (NH_3). Herein, we for the first time demonstrate outstanding performance of MOF-808 for removal of toxic chemicals in humid environment *via* special design of functionalization of hydroxo species bridging Zr-nodes using a triethylene-diamine (TEDA) to form ionic frameworks by gas phase acid-base reactions. *In situ* experimental analyses and first-principles density functional theory calculations unveil underlying mechanism on the selective deposition of TEDA on the Zr-bridging hydroxo sites ($\mu_3\text{-OH}$) in Zr-MOFs. The crystal structure of TEDA-grafted MOF-808 was confirmed using synchrotron X-ray powder diffraction (SXRPD). Furthermore, *operando* FT-IR spectra elucidate

* Corresponding author at: Research Center for Nanocatalysts, Korea Research Institute of Chemical Technology (KRICT), Jang-dong, Yuseong, Daejeon 34114, Republic of Korea.

** Corresponding authors.

E-mail addresses: sgryu@add.re.kr (S.G. Ryu), sjookim@ajou.ac.kr (S.-J. Kim), bchan@yonsei.ac.kr (B. Han), ykhwang@kRICT.re.kr (Y.K. Hwang).

¹ These authors contributed equally to this work.

why the TEDA-grafted MOF-808 shows by far superior sorption efficiency to other MOF varieties. This work provides design principles and applications how to optimize MOFs for the preparation for versatile adsorbents using diamine grafting chemistry, which is also potentially applicable to various catalysis.

1. Introduction

Efficient and safe protection of our environment against chemical warfare agents (CWAs) and toxic industrial chemicals (TICs) has always been an emergent and challenging issue (Munro et al., 1999; Barea et al., 2014). Among CWAs and TICs, cyanogen chloride (CNCl, CK) and ammonia (NH_3) are the archetype representatives, requesting for special attention due to their ubiquitous utilization as base chemicals in a wide range of industrial processes but with the risk of accidental emission in the chemical facilities. It is well known that CK can be lethal even for a short exposure due to its serious damaging to human body's function to use oxygen. Scientific and engineering sectors have made considerable efforts to discover highly efficient materials for adsorptive removal of the toxic hazardous chemicals. For example, activated carbon modified with nucleophilic molecules and metal species such as Cu, Zn, Cr, Mo and Ag, metal oxides, polyoxometalates, and polymer resins were developed (Mahle et al., 2010; Peterson et al., 2010; Mizrahi et al., 2010; Purohit et al., 2014). Nevertheless, innovative design principles and materials are largely missing. It is partly due to serious degradation of active sites and sorption capacities of the materials are seriously degraded, especially, when the materials are exposed to humid conditions (Peterson et al., 2010).

Recently, **Metal-organic frameworks (MOFs)** (Yaghi et al., 2003) have been extensively studied for promising candidates for removing toxic chemicals (Padial et al., 2013; Zhang et al., 2018). It is particularly ascribed to unique properties for gas sorption (Rosi et al., 2003; Yoon et al., 2017; Kaye et al., 2007), separation (Couch et al., 2009; Liu et al., 2018; Li et al., 2009), sensing (Kreno et al., 2012) and catalysis (Lee et al., 2009; Farriseng et al., 2009; Valerkar et al., 2016), such as inherently high porosity, tunable pore size, easy surface functionalization and flexible framework. Among those candidates, zirconium-based MOFs (Zr-MOFs) have been of interest due to additional beneficial features to conventional ones: high thermal, mechanical and chemical stabilities, defect evolutions in metal nodes and ligand sites with a simple modulation process (DeCoste et al., 2015; Platero-Prats et al., 2017; Yang et al., 2018). It was discovered that the surface structures can be optimized by metals and linkers for decomposition or adsorption of toxic chemicals, which are fascinating for not only the scientific community but also industrial sectors (Yang et al., 2011). Some Zr-MOFs showed high performance in the removal of toxic compounds such as benzene and NO in humid conditions (Xie et al., 2018). In functionality control, the topological connectivity between Zr-nodes as a secondary building unit (SBU) and the linkers of organic ligands was identified as the key descriptors for controlling the net frameworks of associated Zr-MOFs. Typically, $\text{Zr}_6(\mu_3\text{-O})_4(\mu_3\text{-OH})_4$ nodes in the framework of Zr-MOFs (UiO-66 series, NU-1000 and MOF-808) are observed as connected with carboxylate linkers of various coordination numbers (6, 8, 10 and 12).

The pore accessibility of the materials, however, can be significantly different even for given topology and surface functional group. For example, UiO-66 series are connected with 12 organic linkers, but NU-1000 series have eight coordination number while MOF-808 series do only six directly attached linkers, and their catalytic activities towards the decomposition of toxic organophosphorus simulants are very dissimilar (Moon et al., 2015). Interestingly, the post-synthetic modification (PSM) was known as a versatile tool for fabricating MOFs with identical topology but diverse functionalities without losing the structural stability (Cohen, 2010; Peng et al., 2018). Some of our authors, indeed, invented the functionalization of metal nodes, located at coordination unsaturated sites (CUS) in MOF, with amines through

covalent bond. Li et al. reported selective grafting of TEDA onto MIL-101 in a similar manner (Hwang et al., 2008; Li et al., 2017). Furthermore, Kim et al. also showed that zirconium tribridged oxo species in metal node of Zr-MOFs can be replaced with Ti and Hf and indeed materialized the idea in UiO-66 s (Kim et al., 2012). Recently, the PSM process is widely utilized for cluster metallization and ligand migration into Zr-MOF to incorporate heterogeneous metal (II) ion, leading to a bimetallic MOF of 8-connected Zr6 node with organic linkers (Yuan et al., 2015; Peng et al., 2016). Li et al. introduced ethylenediaminetetraacetate (EDTA) into MOF-808 in a facile way by exchanging EDTA with the ligand of the original formate group, which is anchored at the Zr metal nodes (Li et al., 2019). Very recently, Yang et al. demonstrated that surface structures of the Zr6 node containing hydrogen-bonding OH and H_2O groups in 8-connected NU-1000 and 12-connected UiO-66 can be activated by methanol (Yang et al., 2016). Another PSM approach to improve the Zr-MOFs performance was replacing of coordinated carboxylic acids by solvent-assisted ligand incorporation (SALI) method (DeCoste et al., 2015). It was, however, reported that the method does not always directly functionalize the Zr-bridging hydroxo sites ($\mu_3\text{-OH}$) in Zr-MOFs. Thus, the rigorous and innovative design principles to empower MOFs to obtain desired performance should be developed, probably from the molecular level aspect of the Zr-node containing $\mu_3\text{-OH}$ sites.

2. Experimental

2.1. Materials preparation

All materials were prepared by reported elsewhere with a little modification. The phase purity of the all materials was confirmed by PXRD. Detailed material characterization was introduced in Note S1-S5, Supporting Information.

Grafting of TEDA onto the samples was performed using the vapor deposition system depicted in Fig. S1. Prior to depositing the TEDA, 1 g of sample was placed into a 10 mm i.d. fritted quartz reactor and activated at 423 K for 6 h in flowing dry helium (20 mL min^{-1}). Subsequently, the helium flow was shut off and a 30 mL stainless-steel bulb containing a target amount of TEDA was connected to the system. The reactor outlet was connected to a cold trap to collect undeposited gaseous TEDA by recrystallization. Concurrent sublimation of TEDA and its deposition onto the samples, were conducted by increase of the bulb temperature at a ramping rate of 1 K min^{-1} from room temperature to 423 K under vacuum (10^{-2} torr). The system was further maintained at 423 K for 1 h, and then cooled to room temperature under helium flow.

2.2. Breakthrough testing

All were pressed into pellets using an Enerpac Press and 3.1-cm die corresponding to pressures of 100 bar. The pellet crushed and sieved to yield 60×70 mesh particles, which were forwarded for breakthrough testing. An apparatus schematic of the breakthrough test system can be found in Fig. S2. Next, 50 mm^3 of sorbents was loaded onto the test bed in a 4.0 mm i.d. glass tube reactor. For humid condition testing, sorbents were pre-humidified at 293 K for 2 h at the 80 % relative humidity in a flowing air. The CK was delivered to a bulk flow of either dry or humidified air to achieve the target challenge concentration (4000 mg/m^3). The breakthrough test was conducted with 20 mL min^{-1} of branched flow from the bulk flow of the mixture at 297 K and atmospheric pressure. Concentration of the effluent gas from the

reactor was measured using an online gas chromatograph (Agilent 7890B) equipped with a flame ionization detector (FID). Breakthrough curves were plotted on a normalized time scale of minutes per gram of sorbent to account for difference in density. The end point (breakthrough concentration) was evaluated at 5 mg m^{-3} by military toxic exposure limits for CK. The adsorbed amount of CK was calculated using the adsorption time to the breakthrough concentration. Detailed test parameters were summarized in Table S1. For the other toxic gases, DMMP and ammonia were tested with the same apparatus, but the concentration of the effluent DMMP was measured using an online gas chromatograph (Agilent 7890B) equipped with a flame photometric detector and the outlet concentration of ammonia was analyzed using online tunable diode laser adsorption spectroscopy gas analyzers (Airwell +7). The initial concentration of DMMP and ammonia was 3000 and 1000 mg/m^3 , respectively, and the other breakthrough testing parameters for DMMP and ammonia were summarized in Table S2 and S3.

3. Results and discussion

3.1. Direct functionalization of Zr-based MOF node

MOF-808 or $\text{Zr}_6(\mu_3\text{-O})_4(\mu_3\text{-OH})_4(\text{BTC})_2(\text{HCOO})_6$ was built from Zr-based SBU of $\text{Zr}_6(\mu_3\text{-O})_4(\mu_3\text{-OH})_4$ node consisting of connected network of 1,3,5-benzentricarboxylate (BTC) linker and six formate (HCOO) balancing electric charge to form 3-dimensional porous framework (Fig. 1a). There are two different types of pores: tetrahedral and adamantane cage. The former is inaccessible by guest molecules due to its small aperture diameter of 1.2 \AA , while the latter forms much larger diameter of 18.4 \AA . To achieve the selective functionalization of hydroxo bridged Zr-OH-Zr species on the MOF-808, triethylenediamine (TEDA) was selected as an effective grafting agent with multifunctional chelating groups (detailed preparation is provided in the Supporting Information, Note S2). In this structure, the $\text{Zr}_6\text{-oxo}$ cluster has four adsorption sites such as $\mu_3\text{-OH}$, $\mu_3\text{-O}$, $-\text{HCO}_2$, and BTC linker configured after thermal treatment at 423 K . If one of the amine groups in the

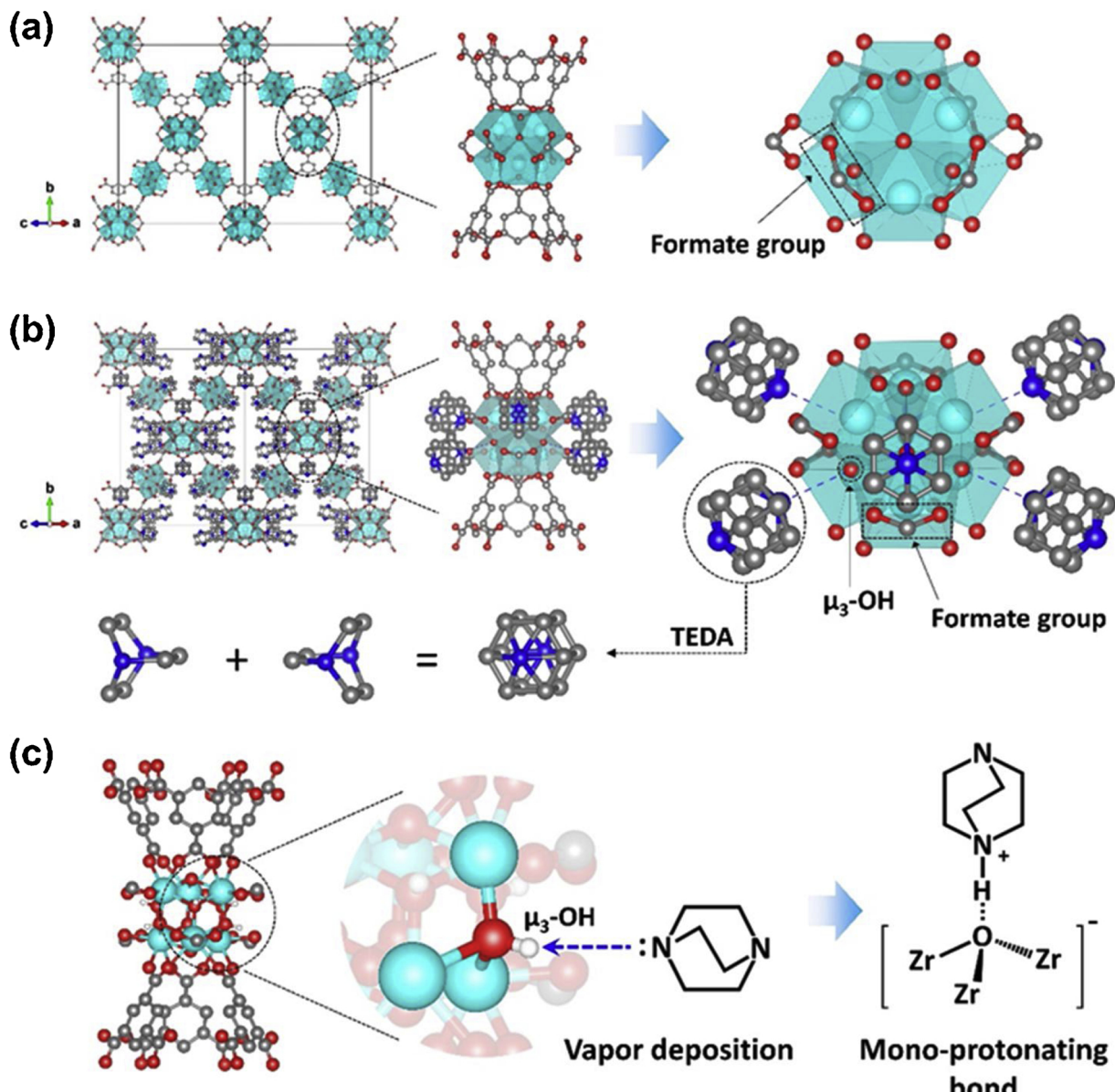


Fig. 1. Comparison of crystal structures of (a) MOF-808 and (b) T-MOF-808. The polyhedral represent ZrO_8 group. Atom colors are Zr: cyan, C: dark gray, O: red and N: blue. Water molecules were excluded. In the structure of T-MOF-808, the TEDA molecules were allowed to be superimposed as a result of molecular rotations. (c) Schematic representation of TEDA (triethylenediamine) functionalization of MOF-808.

TEDA selectively interacts with $\mu_3\text{-OH}$ via acid-base reaction, the rest can play their intended function (adsorption for toxic chemicals). It should be noted that this design concept was not applied to the surface functionalization of Zr-based SBU of $\text{Zr}_6(\mu_3\text{-O})_4(\mu_3\text{-OH})_4$ node yet. Hereafter, TEDA-loaded MOF-808(Zr) will be noted as T-MOF-808.

3.2. Spectroscopic evidence and DFT calculations for grafted TEDA on Zr nodes

FT-IR spectra clearly demonstrate that TEDA was selectively grafted on $\mu_3\text{-OH}$ group in Zr cluster on MOF-808 (Fig. 2a). As TEDA contents increases to 8 wt% a strong band at 3674 cm^{-1} , which describes the stretching vibration mode of *tri*-bridged OH species in $\text{Zr}_6(\mu_3\text{-O})_4(\mu_3\text{-OH})_4$ node (Shearer et al., 2013), gradually disappears. With more than 30 wt% of the grafting of TEDA in MOF-808 the peak completely fades out. It means that the $\mu_3\text{-OH}$ sites were almost saturated with the deposited TEDA. Simultaneously, the intensity of a narrow peak at 1054 cm^{-1} , which is the characteristic vibration mode of $\nu_{\text{as}}(\text{NC}_3)$ in TEDA, increased and then, saturated in the opposite manner of the $\mu_3\text{-OH}$ does. The theoretical amount of the $\mu_3\text{-OH}$ group calculated from the MOF-808 $\text{Zr}_6(\mu_3\text{-O})_4(\mu_3\text{-OH})_4(\text{HCOO})_6(\text{BTC})_2$ cluster was approximately $2.93\text{ mmol/g}_{\text{MOF}}$, which well agrees with the elementary analysis (EA) for the grafted one with 30 wt% TEDA (loading of 2.68 mmol/g). Several additional vibrational bands further demonstrate the characteristic peaks of the metal nodes, linkers and TEDA. For examples, a broad band in a range of $3600\text{--}3100\text{ cm}^{-1}$ is from adsorbed water molecules in pores, which is hydrogen bonded to probably hydroxyl group and aqua ligands in MOF-808. Vibrational bands in ranges of $3100\text{--}2700\text{ cm}^{-1}$ are ascribed to the well-known C-H stretching modes associated with mono carboxylic acid ($\nu_s(\text{C-H}) = 2932\text{ cm}^{-1}$, $\nu_{\text{as}}(\text{CH}) = 2866, 2744\text{ cm}^{-1}$). Also, the result shows extra peaks ($\nu(\text{C=O}) = 1100\text{ cm}^{-1}$, $\delta(\text{OH}) = 940\text{ cm}^{-1}$). As increasing TEDA contents the vibration mode of formate in a range of $3100\text{--}2700\text{ cm}^{-1}$ tends to shift to lower wavenumbers due to the perturbation with C-H stretching mode in TEDA.

Moreover, first-principles density functional theory (DFT) calculations also figured out underlying mechanism on why the TEDA should be selectively deposited on $\mu_3\text{-OH}$ group in MOF-808. Calculated adsorption energies of TEDA (the more negative value is the more plausible thermodynamically) on four different sites ($\mu_3\text{-OH}$, $\mu_3\text{O}$, H—CO₂, and BTC linker) in MOF-808 were summarized in Fig. 2b. It indicates that the adsorption energies are very heterogeneous depending on the adsorption sites of the metal/organic building unit. A TEDA molecule evidently prefers $\mu_3\text{-OH}$ site (-0.52 eV) rather than others (~ -0.22 eV). We determined that the van der Waals interaction plays a role in the adsorption of TEDA at $\mu_3\text{-O}$, H—CO₂, and at the BTC

linker, while $\mu_3\text{-OH}$ binds to TEDA more strongly. This implies that TEDA is selectively adsorbed to the $\mu_3\text{-OH}$ site during the vapor deposition process and because of the high protonating ability of $\mu_3\text{-OH}$ TEDA, will undergo acid-base reaction to bind even more tightly.

To investigate thermodynamic stability of the T-MOF-808 as a function of grafted TEDA content, we calculated tethering energy of TEDA with respect to its loading (as wt% or the number of TEDA molecule) as shown in Fig. S3. In T-MOF-808 model, there are 16 $\mu_3\text{-OH}$ sites and 12 $\mu_3\text{O-H}$ sites were considered as TEDA adsorption sites available (around 25 wt%) because four $\mu_3\text{-OH}$ sites are in the tetrahedral cavities. Our results clearly pose that the tethering energy shifts from negative to positive value (*i.e.* weaker binding) as the number of adsorbed TEDA increases. It can be explained by the steric hindrance effect on the adsorption energy. Nevertheless, the tethering energy is still negative (-0.32 eV) at TEDA loading of 24.68 wt% implying that the $\mu_3\text{-OH}$ sites of the MOF-808 selectively adsorb a large amount of TEDA molecules.

To understand the chemical change of $\mu_3\text{-OH}$ caused by the protonation of TEDA (Guzonas and Irish, 1988; Pirc et al., 2012), samples of TEDA, di-protonated TEDA, 30 %T-MOF-808 and MOF-808 were carefully analyzed using FT-IR, Raman and solid state nuclear magnetic resonance (NMR) spectroscopy (Fig. 3). Among the protonated forms, a mono-protonated TEDA is the most plausible configuration (Fig. S4). It is formed by a series of processes that one of initial step of the TEDA protonation is the anchoring of TEDA at the $\mu_3\text{-OH}$ site, in which thermodynamic stability of the TEDA is degraded as its number increases. By the loading process, the TEDA exists as the two nitrogen groups in TEDA strongly binds to $\mu_3\text{-OH}$ and then, breaks the O-H bonding by forming a new N⁺H species (Fig. 1c). It was apparently believed that additional protonation mechanism is unlikely since the sample is pre-treated at 423 K for 12 h followed by evaporation of the TEDA at the same temperature under primary vacuum condition. In addition to N⁺H stretching mode, bending vibration mode of $\delta(\text{N}^+\text{H}) = 1250\text{--}1450\text{ cm}^{-1}$ was observed in T-MOF-808. Raman spectra further proved the existence of N⁺H species, and broad bands of $\delta(\text{N}^+\text{H}) = 1250\text{--}1450\text{ cm}^{-1}$ appear in di-protonated TEDA (Fig. S5). When it compares to N⁺H vibrational modes, there were small band shifts and the intensity changes in $350\text{--}1200\text{ cm}^{-1}$ region, associated with variation of NC₃ bond angles due to protonation of TEDA. Furthermore, additional two protons affect both the mass of the nitrogen atoms and the distribution of bonding electrons. It results in shifts to lower wavenumbers ($\delta_{\text{as}}(\text{NC}_3)$; bare TEDA = 428, 580 cm⁻¹, 30 %T-MOF-808 = 418, 572 cm⁻¹, di-protonated TEDA = 415, 562 cm⁻¹) (Fig. 3b).

Nuclear magnetic resonance (NMR) spectroscopy is one of the most sensitive techniques to detect changes in the electronic environment of the carbon and hydrogen groups (Cralk and Levy, 1982). Here, solid

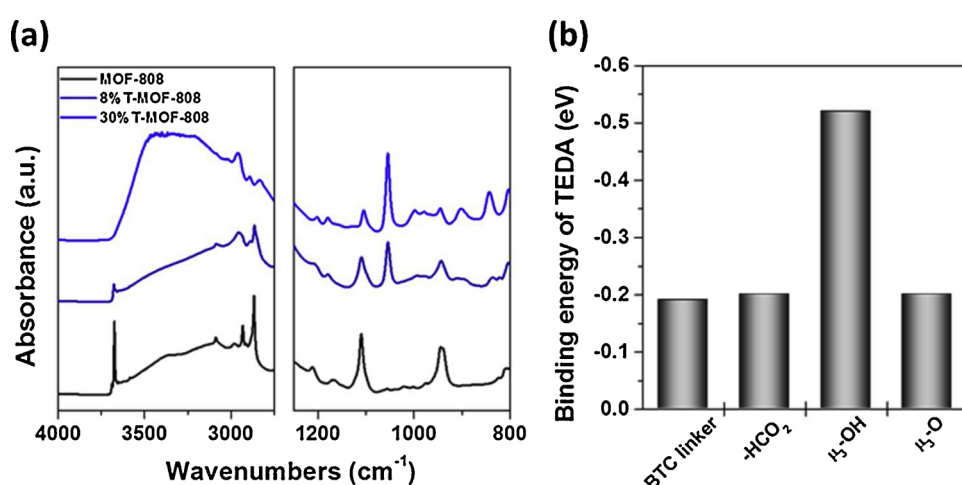


Fig. 2. (a) FT-IR spectra of MOF-808 and TEDA loaded MOF-808 under He flows and (b) adsorption energy of TEDA in MOF-808.

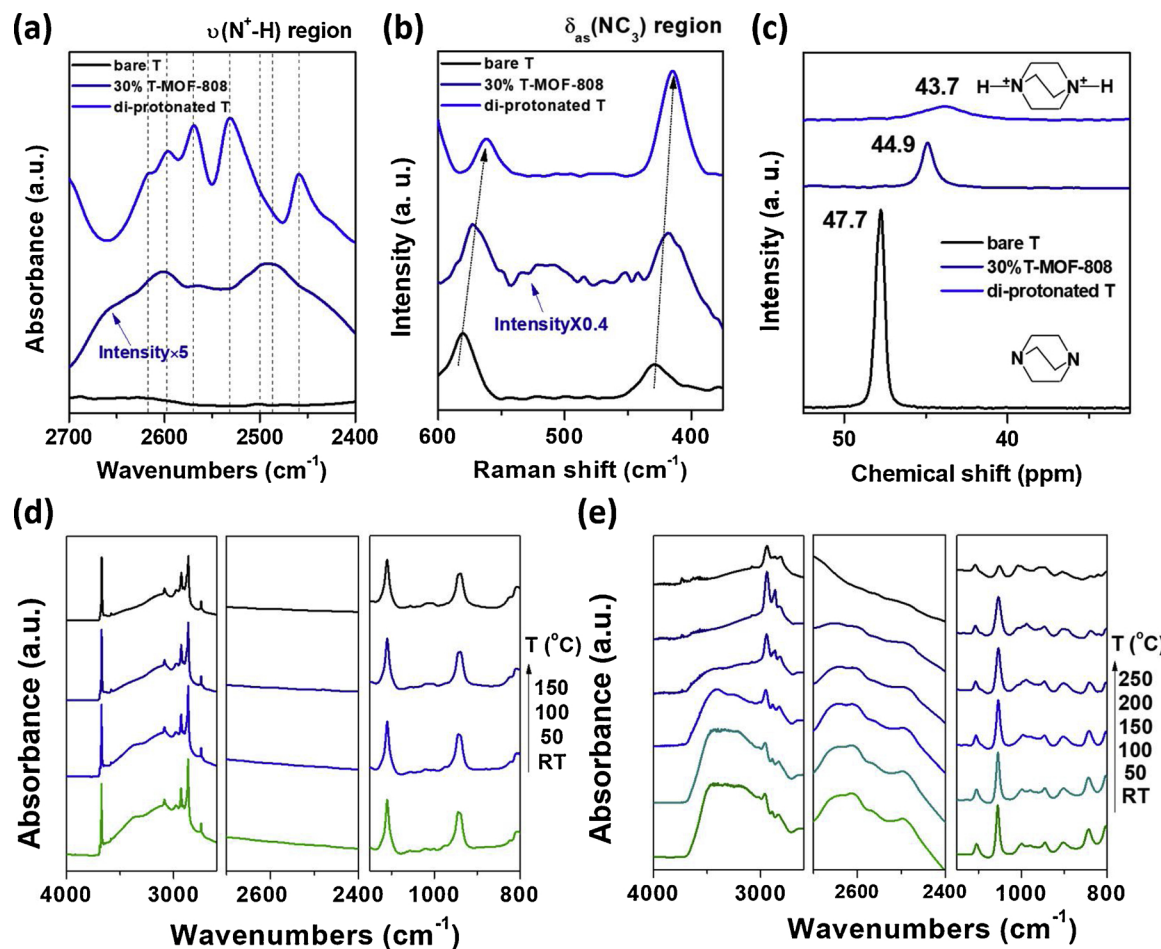


Fig. 3. (a) FT-IR, (b) Raman spectra, (c) Solid state ^{13}C NMR of bare TEDA, 30 %T-MOF-808 and di-protonated TEDA and temperature-dependent *in-situ* FT-IR spectra; (d) MOF-808, (e) 30 %T-MOF-808 under He flows.

state NMR was further fulfilled to confirm the nature of TEDA species grafted on MOF-808. In Fig. 3c and S6, ^{13}C NMR chemical shifts of T-MOF-808 were observed in 170.0 ($\text{C}=\text{O}$), 135.8 (quaternary aromatic carbon), 130.0–120.0 (C–H broadening) from MOF-808 and 44.9 ppm from TEDA (Peterson et al., 2010), which was definitely located in between di-protonated TEDA (43.7 ppm) and TEDA (47.7 ppm). It can be ascribed to the fact that bonding type of TEDA at tri-bridged OH of MOF-808 is mono-protonated. It is because that the removal of lone pair electrons and protonation induce an upfield chemical shift. The chemical shift profiles of protonated T-MOF-808 is similar to that of the ethylenediamine grafted Y zeolites *via* conjugated acid-base formation (Kim et al., 2016). In contrast to the observations of the ^{13}C chemical shifts, ^1H shifts moves downfield upon the protonation process (Fig. S7). ^1H chemical shifts of TEDA grafted MOF-808 have been measured in 8.5 (BTC linker), 8.0 (formate), 4.8 (TEDA, closely linked to $\mu_3\text{-OH}$), 2.6 (TEDA, located apart from $\mu_3\text{-OH}$) ppm (Moon et al., 2015). The values of ^1H chemical shifts of TEDA are located at the midpoints when it compared to bare (2.2 ppm) and di-protonated (3.5, 5.3 ppm) TEDA species.

3.3. Structure, texture properties and thermal stability of T-MOFs

The X-ray diffraction patterns (XRD) of T-MOF-808 was almost the same as the pristine MOF-808, with slight change of the Bragg intensities, implying that TEDA grafting does not affect the crystallinity (Fig. S8) (Furukawa et al., 2014). This result is consistence with previous reports (Hwang et al., 2008) showing no apparent loss of crystallinity due to the incorporation of diamine in the pores of MOFs and it

implies that the TEDA is successfully deposited on specific sites in the large pores of MOF-808. Since MOFs are generally constructed by co-ordination bonds between metal-ion and dicarboxylic acid ligand, frameworks can be easily broken by basic molecules (such as TEDA) in solution (Howarth et al., 2016; Yuan et al., 2018). It is noteworthy that the deposition of basic molecules in gas phase can minimize the structural degradation of MOF, due to selective positioning at specific sites of MOF.

To precisely investigate crystal structure of T-MOF-808, we performed the synchrotron X-ray powder diffraction (SXRPD) analysis (CCDC 1944768). As shown in Fig. 4a, all diffraction peak position of the T-MOF-808 are consistent with a cubic structure (space group $Fd\bar{3}m$) with a lattice parameter $a = 35.45489(9)$ Å. The unit cell volume of the T-MOF-808 is about 1.5 % larger than that of a pristine MOF-808. Our SXRPD measurements indicates that the $\text{Zr}_6(\mu_3\text{-O})_4(\mu_3\text{-OH})_4$ units linked with BTC ligands was preserved. It is noteworthy that diffraction peaks, such as (111), (311), and (222), for the T-MOF-808 looked different from calculated patterns considering only atomic coordinates (except for H-atoms) of the $[\text{Zr}_6(\mu_3\text{-O})_4(\mu_3\text{-OH})_4(\text{HCOO})_6(\text{BTC})_2(\text{H}_2\text{O})_{12}]$ without TEDA ligands (Fig. 4b). The differences significantly decreased when TEDA ligands were incorporated at the positions determined from the DFT calculations and additional water molecules in the adamantine cage inside the framework (Fig. 4c). The final chemical formula used in the refinement was $[\text{Zr}_6(\mu_3\text{-O})_4(\mu_3\text{-OH})_4(\text{HCOO})_6(\text{BTC})_2(\text{TEDA})_4(\text{H}_2\text{O})_{40}]$. The water content was consistent with the weight reduction observed in the temperature range of 300–400 K in TGA experiment (Fig. S9). In the refinement process, TEDA molecule was considered individually as a

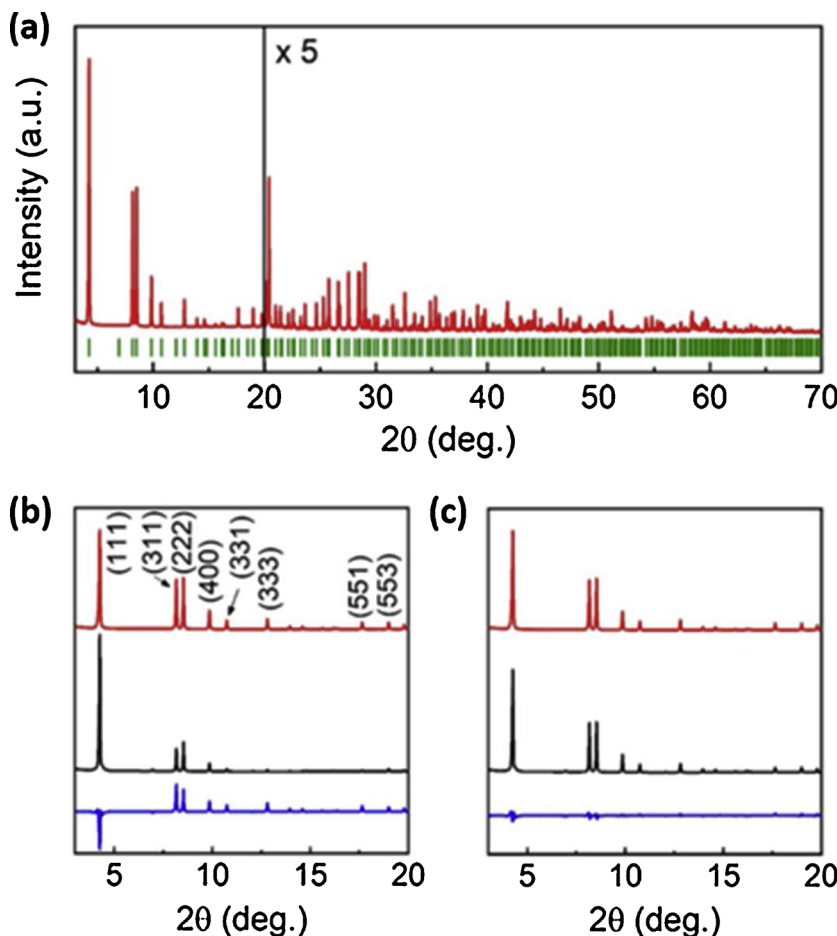


Fig. 4. (a) A synchrotron X-ray diffraction pattern for the 30 % T-MOF-808. Bragg positions are indicated by the green vertical markers. The fitting results based on the model without TEDA ligand in (b) and with considering TEDA ligand in (c). The red lines correspond to observed data and black lines show calculated patterns based on each of the models, while blue lines at the bottom denote differences between the observed and calculated.

rigid body and its geometry was built from ideal interatomic distances of C–C (1.54 Å) and C–N (1.48 Å) bonds. The TEDA molecules were allowed to be superimposed as a result of molecular rotations and partially occupy the crystallographic sites. For 30 % T-MOF-808, the total number of TEDA molecules per formula was constrained to be four, i.e., the N and C atoms were statistically distributed over their sites with occupancies of 67 % and 33 % on average.

The positions of oxygen atoms in water molecules were determined from the difference Fourier map calculations. The summary of crystallographic data is listed in Table S4. The schematic structure determined from SXRPD is presented in Fig. 1b, which shows that TEDA is grafted on μ_3 -OH site. The refinement result indicates that the overall linkages between $Zr_6(\mu_3\text{-O})_4(\mu_3\text{-OH})_4$ nodes and BTC ligands remain unchanged after TEDA grafting, but the formate group shift to new position where the formate binds to only one Zr atom forming a chelate structure. The positional shift of formate group is thought to be a result minimizing the repulsion with the grafted TEDA ligands. After TEDA grafting, both surface area and pore volume decreased due to the anchored TEDA at the pores (Fig. S10).

Compared to the pristine MOF-808, the T-MOF-808s exhibit moderate decrease for the adsorption of N_2 at $P/P_0 > 0.01$. The BET surface area decreases from 1612 to 1024 m^2/g after grafting. The pore size distribution (PSD) profiles calculated by DFT show a gradual change in the pore sizes of MOF-808 after TEDA grafting, probably due to selective loading on tri-bridged OH sites from 8 wt% to 30 wt% TEDA, giving rise to changing PSD from 1.86 nm to 1.59 nm. The textural properties of the pristine and TEDA grafting samples and amount of loaded TEDA estimated by the elemental analysis (EA) are summarized in Table S5.

The stability of the TEDA modified MOF-808 frameworks was investigated using a thermal gravimetric analysis (TGA) (Fig. S9). The weight loss up to 373 K was attributed to adsorbed water molecules

attached to pores, and then gradually decreased up to 623 K by removal of formate groups and BTC linkers associated with deposited TEDA. The TEDA were not totally removed even when it was heated over than 423 K, consistent with the assumption of strong interaction between TEDA and MOF-808 surface. Temperature dependent *in situ* FT-IR spectra were further confirmed to prove the thermal stability of the TEDA grafted MOF-808. As shown in Fig. 3d and e, tri-bridged OH group in MOF-808 is stable up to 423 K, which is, in fact, the deposition temperature of gas phase TEDA. It clearly reveals that TEDA is deposited at μ_3 -OH site with strong chemical bonding represented by the peak (v_{as} (NC_3) = 1054 cm^{-1}) at higher than 473 K. As shown in Fig. 3e, the protonated TEDA anchoring to the μ_3 -OH of MOF-808 uptake the H_2O molecules well, and the added H_2O can participate in the hydrolysis reaction of CK. In addition, the peaks of TEDA bound to MOF-808 ($v_s(N^+H)$ = $2500 - 2700\text{ cm}^{-1}$) do not completely disappear even at 473 K.

3.4. Sorption characteristics and operando FT-IR investigation of T-MOFs

TEDA modified MOFs such as UiO-66, mesoporous MIL-100/101 and MOF-808 along with commercial T-ASZM, and zirconium oxyhydroxide were examined to measure sorption abilities for toxic chemicals. We tested their performances towards cyanogen chloride (CK), which is a highly toxic blood agent, and one of the most difficult CWAs to remove in the humid environment (Glover et al., 2011). It is noteworthy that sorbents for removal toxic gases should have at least a threshold level of protection as the first responders upon exposure (DeCoste and Peterson, 2014). In case of CK, the end point concentration should be below $5\text{ mg}/m^3$. It is well known that metal (Ag, Cu, Zn, Mo, and etc.) and TEDA impregnated T-ASZMs are typically used as

adsorbents for CK removal. Breakthrough curves of CK under dry and humid conditions (RH 80 %) were illustrated in Fig. 5, and Table 1 summarized the calculated adsorbed amount of CK at the end point. In dry atmosphere (Fig. 5b), mesoporous T-MIL-101 and T-MOF-808 show similar breakthrough time, indicating that TEDA can facilitate the removal of CK in a stoichiometric manner.

As shown in Fig. 5c, however, T-MOF-808 shows superior removal efficiency (4.05 mmol/g) to others, T-Uio-66 (2.38 mmol/g) and T-MIL-100 (0 mmol/g), T-MIL-101 (0 mmol/g) as well as ZrO(OH)₂ (1.28 mmol/g) and T-ASZM (1.19 mmol/g) in humid environment (RH 80 %). As expected from previous literature (Peterson et al., 2013), Zr-based MOFs, T-Uio-66 and T-MOF-808 remove larger amounts of CK in humid conditions than in dry environment. It is consistent with the fact that the removal efficiency of basic Zr(OH)₄ for CK is enhanced by impregnated TEDA (Peterson et al., 2010). It should be noted that the humidity plays a very important role in the removal of CK. Previous studies (Mahle et al., 2010) proposed that protonation of TEDA by water and humid generates hydroxyl ion (OH⁻), which then hydrolyzes CK and yields other by-products as well as promoting the CK hydrolysis.

In general, it is known that grafting of impregnants deposited on the surface of a typical sorbent is limited by steric hindrance effect (Hwang et al., 2008). On the other hand, Zr-MOFs are highly porous materials with large pore sizes and induced defects due to missed linkers, a large amount of TEDA can be deposited without clogging pores. Note from Fig. 5a, that the CK removal capacity was promoted as increasing the TEDA content. Here, Uio-66 and MOF-808 as well as mesoporous MIL-101 and MIL-100 with maximum amounts anchored TEDA from its excessive vapors have been tested for CK removal. Of these, the 30%T-

Table 1

Surface area (S_{BET}), total pore volume and adsorbed amount of CK of MOF materials.

Materials	Loading amount of TEDA		S_{BET} (m ² /g)	V_{total}^a (ml/g)	ρ_{bulk}	Adsorbed amount of CK ^b (mmol/g)	
	(wt %)	(mmol/g)				Dry	Humid
T-ASZM	8	0.71	857	0.48	0.55	1.07	1.19
T-MOF-808	30	2.68	1024	0.49	0.50	1.26	4.05
T-Uio-66	20	1.79	536	0.64	0.31	1.43	2.38
T-MIL-100	24	2.15	926	0.40	0.49	0.31	0
T-MIL-101	30	2.67	2616	1.30	0.20	1.78	0
T-ZrO(OH) ₂	8	0.71	229	0.17	0.92	1.19	1.28

^a Total pore volume was calculated at $P/P_0 = 0.95$.

^b Adsorbed amount of CK was calculated from breakthrough point ([CK] = 5 mg/m³). All the CK breakthrough tests in humid conditions were performed at RH 80 %.

MOF-808 material was measured to have the longest breakthrough time, as well as the highest sorption capacity for CK (Fig. 5).

Although evaluated Zr-MOFs have the same SBUs as Uio-66, the molecular connectivity of each node is different. Unlike the small apertures of Uio-66, (12-connected), the MOF-808 (6-connected) offers remarkably larger ones (or windows), and facilitates the delivery of CK to inside of the framework. As a result, a much more nodes can be utilized for adsorption sites of CK (Moon et al., 2015). In addition, once it was activated as removing formate, zirconium sites can be less crowded with linkers and a great number of adsorbed water molecules

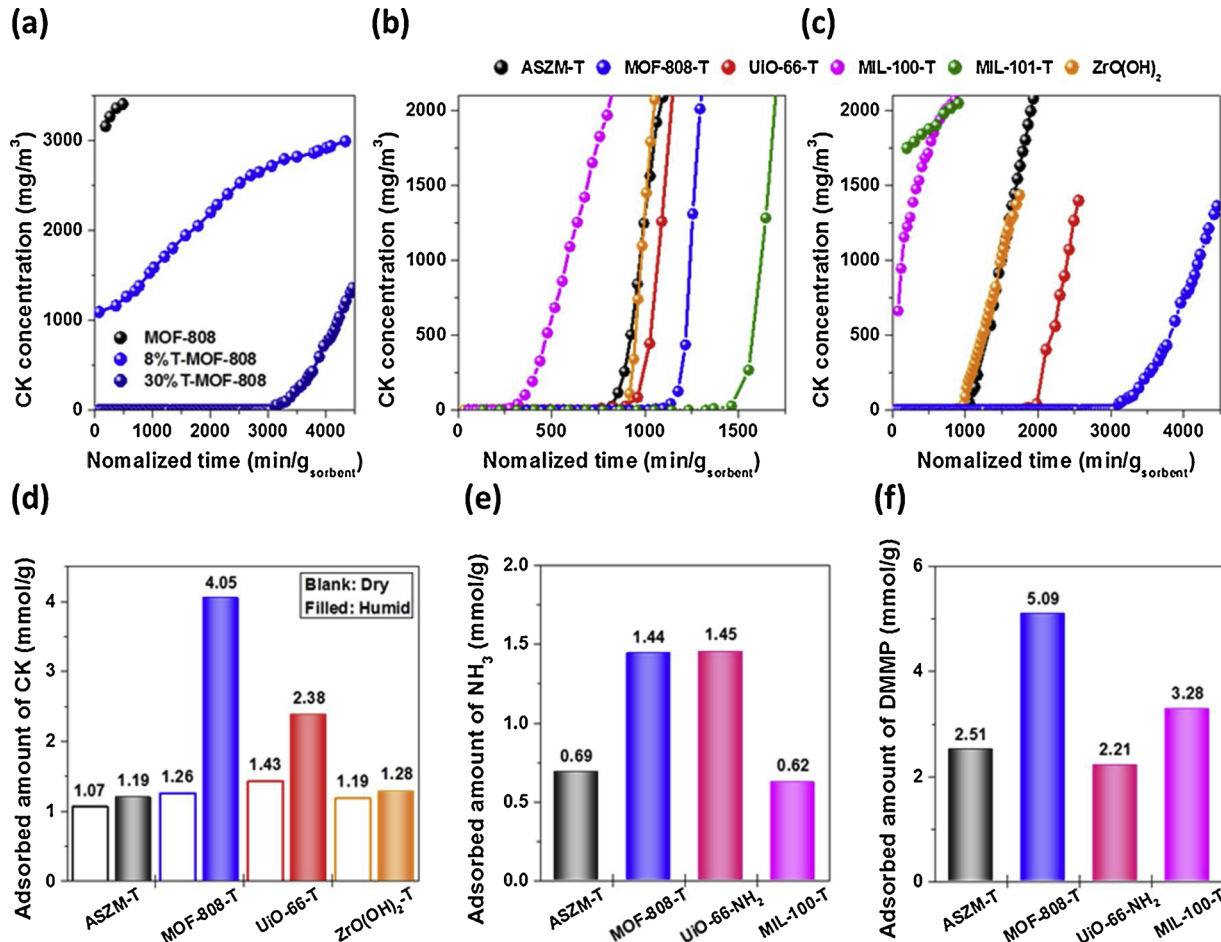


Fig. 5. CK breakthrough of TEDA loaded adsorbents; (a) MOF-808 with various TEDA contents, all materials under (b) dry, (c) conditions (RH 80 %), and adsorption performance is shown in panel (d) CK, (e) NH₃ and (f) DMMP.

are contained in MOF-808 (Moon et al., 2015). Furthermore, Zr-MOFs possess both acidic and basic sites; the quantity of these sites are much more in MOF-808 than in UiO-66(Zr) (Valerkar et al., 2016). The origin of the acid-base sites was from Zr–OZr or ZrOHZ—r bonding clusters in the metal nodes of the Zr–MOFs, which possess strong binding sites for decomposed CK of HCl and HOCl under humid environment. It should be noted that the target gases in this study are chemical warfare agents, which are generally used for military respiratory purpose. Therefore, adsorbent used for CWAs removal are not used for cyclic utilization due to contamination of adsorbent with toxic chemicals and their decomposed products.

Operando FT-IR investigation revealed a substantial formation of CK and by-products on the surface of TEDA grafted Zr-MOFs. The IR spectra were monitored in dry and humid environments. As shown in Fig. 6c, the modes at 2207 cm^{-1} assigned to $\nu(\text{CN}\equiv)$ of CK adsorbed in mono-protonated TEDA increased its intensity as the exposure to CK increases. The modes at 2151 cm^{-1} and 2133 cm^{-1} originated from $\nu(\text{CN}\equiv)$ of cyanate and isocyanate species, respectively. These species were produced by the hydrolysis reaction of cyanic acid and subsequently adsorbed on mono-protonated TEDA in the presence of water.

As the reaction proceeds, hydrochloric acid is generated as a by-product. Accordingly, a broad band of $\nu_{\text{s}}(\text{N}^+\text{H})$ appears at $2500\text{--}2700\text{ cm}^{-1}$ associated with the dissociative adsorption of hydrochloric acid on the mono-protonated TEDA in the T-MOF-808 (Fig. 6b). The presence of adsorption sites, providing a buffer for hydrolysis by-products, can facilitate the reaction of CK according to Le Chatelier's principle. The molar ratio of removed CK per grafted TEDA was calculated about 1.5:1, indicating that TEDA hydrolyze the CK in humid environment, but it is very reasonable to consider the hydrolysis of CK on basic and acidic site of Zr-node of T-MOF-808. In addition, at the intensity of the vibrational modes by CK species in the T-MOF-808 are still retained as strongly as them bound to the mono-protonated TEDA (Fig. S18). On the other hand, the peak intensity of three modes at 2211 cm^{-1} , 2167 cm^{-1} and 2139 cm^{-1} in TZ–rO(OH)₂ marginally decrease after N₂ purging, due to relatively low interaction of CK and its hydrolyzed species, cyanate and isocyanate with the framework of T–ZrO(OH)₂ (Fig. S21). Few changes in C–H vibrational modes of TEDA is attributed to adsorbed water molecules, and it was confirmed as comparing with IR spectra in dry condition (Fig. S15). The IR patterns of dry and humid conditions are quite similar in TEDA loaded MOF-808. It is ascribed to

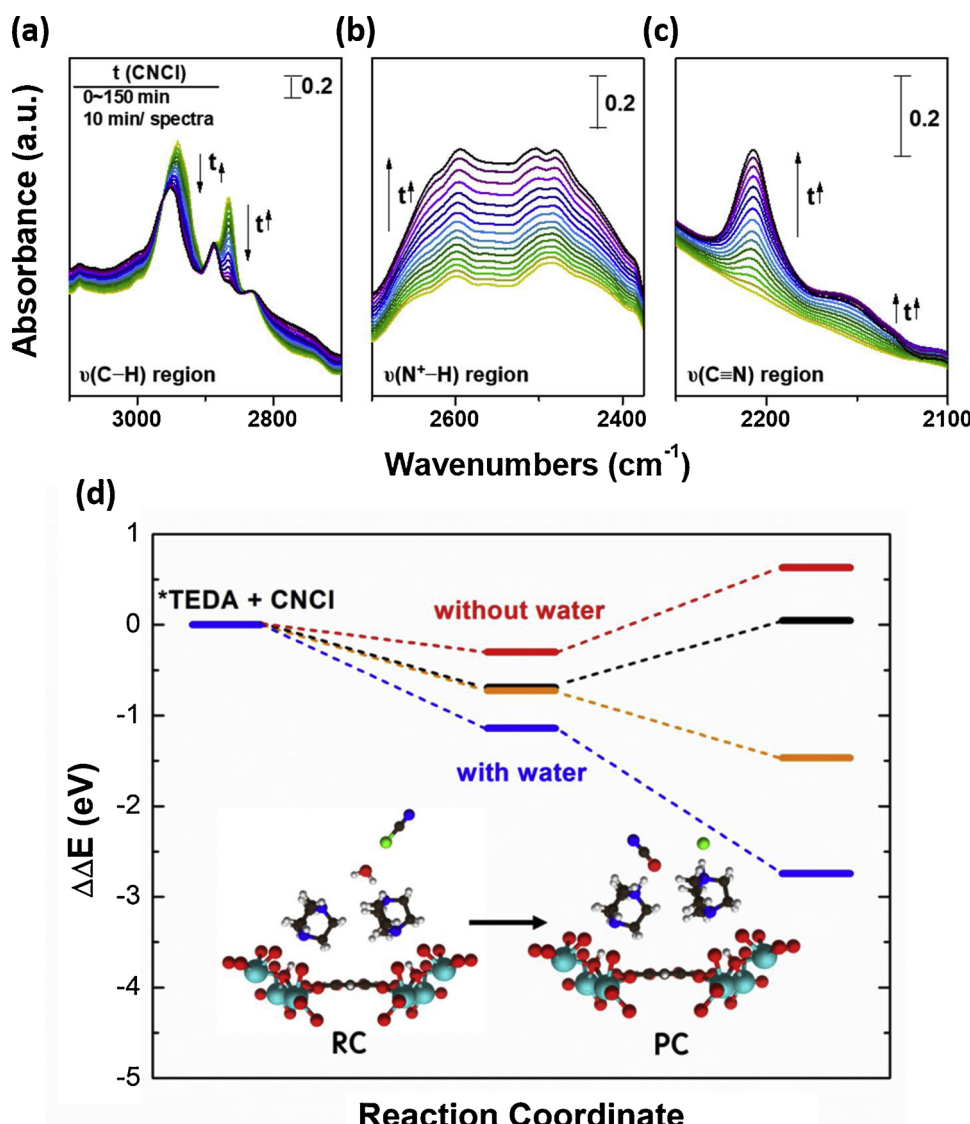


Fig. 6. Operando FT-IR spectra of 30 %T-MOF-808, followed by the introduction of humid reaction gas (CK) does into IR cell at 298 K, (a) $\nu(\text{C}-\text{H})$ region, B) $\nu(\text{N}^+-\text{H})$ region, C) $\nu(\text{CH}\equiv)$ region and (d) Free energy diagram of CK adsorption in T-MOF-808 system (TEDA: orange and black lines and (HTEDA)⁺: blue line in humid conditions). Inset figure represents the schematic figures for reactant complex (RC) and product complex (PC) of CK hydrolysis reaction with TEDA in T-MOF-808 system.

the fact that the MOF-808 still has residual water molecules in the pores after the activation process.

3.5. Adsorption mechanism of CK by DFT calculations

Adsorption mechanism of CK was also investigated by DFT calculations. We calculated adsorption energies of target molecules and expected product species as shown in Table S6. Both CK and H₂O were preferentially adsorbed to N-moiety in TEDA molecule, but adsorption of H₂O was stronger than that of CK, meaning H₂O is favoured by the N-moiety. Interestingly, CK-hydrolyzed products, CNOH and HCl were evaluated as more strongly adsorbed than CK and H₂O. It indicates that hydrolyzed molecules are more easily captured by MOF-808/T-MOF-808 than a pure form of CK.

Experiments proposed that CK underwent two different reaction pathways in T-MOF-808 depending on the humidity levels (Mahle et al., 2010). CK was known to form a salt under vacuum condition, while hydrolyzed structure in the presence of water. In order to distinguish reaction mechanism of CK in T-MOF-808, we calculated a free energy diagram over the adsorption process, as shown in Fig. 6d. It indicates that without water CK molecule does not form a salt with TEDA. On the other hand, TEDA plays a role like a buffer as explained above, leading the CK to react with water to form CNOH and HCl. Then, it was calculated that CNOH and HCl molecules are by far more strongly adsorbed in T-MOF-808 as illustrated in Table S6. Thus, CK easily reacts with water in T-MOF-808 under humid conditions. As shown in Fig. 6d, CK is adsorbed in mono-protonated T-MOF-808 (blue line) shows considerable thermodynamic stability. This is because MOF-808 provides active adsorption site $\mu_3\text{--OH}$ for TEDA.

On the basis of the results we propose that a major role of T-MOF-808 is to facilitate the hydrolysis reaction of CK, not by direct enhancement of the adsorption energy of CK but by attracting H₂O molecule toward N-moiety to provide the stable reactant complex of the CK hydrolysis. Most importantly, the products of CK hydrolysis reactions, CNOH and HCl, are stably adsorbed in the T-MOF-808, by which the removal efficiency is dramatically improved.

To evaluate the multi-functionality of the suggested T-MOF-808 for removing other toxic chemicals we tested the removal efficiency for dimethyl methylphosphonate (DMMP) and ammonia, which are representatives of nerve-agent simulant and toxic industrial gases. Adsorption amount of ammonia and DMMP under humid conditions (RH 80 %, and RH 15 %, respectively) were calculated at the end point (35 mg/m³, 0.04 mg/m³) and results are summarized in Fig. 5e and f. T-MOF-808 shows similar removal efficiency (1.44 mmol/g) to UiO-66-NH₂ (1.45 mmol/g), via interaction with NH₃ through a strong hydrogen bonding (Katz et al., 2015). Moreover, it outperforms the other adsorbents, commercial adsorbent of T-ASZM (0.69 mmol/g) and T-MIL-100 (0.62 mmol/g). Recently, Plonka et al. demonstrated the effective removing ability of DMMP in MOF-808 via *in situ* FT-IR spectra (Wang et al., 2017). As expected, the specific MOFs that have both micro- and mesopore such as MIL-100 and MOF-808 represent a higher DMMP removal performance than the microporous MOFs like UiO-66 and T-ASZM. It should be noted that even if the hydroxide group connected in Zr₆ node is bound to TEDA, T-MOF-808 has superior removal efficiency for ammonia. It can be explained the formate group, which is covalently connected to Zr cluster of MOF-808, can be easily exchanged with water molecule as it activated (Moon et al., 2015). The produced water and hydroxyl ligands make active sites strengthen the hydrogen bonding. Under humid environment, the P=O group of DMMP can interact with O-H group and water through hydrogen bonding, resulting in increased adsorption capacity than dry condition. After the TEDA grafting the concentration of OH group lowered, but TEDA can also function as additional adsorption sites for DMMP. Therefore, it is beneficial to use T-MOF-808 as versatile adsorbents for simultaneous removal of CK, CWAs and TICs, without interrupting the individual removal performance.

4. Conclusions

Here, the strategy to improve the removal efficiencies of cyanogen chloride (CNCl, CK) was implemented through the selective functionalization of Zr-bridging hydroxo sites ($\mu_3\text{--OH}$) on Zr-nodes in MOF-808 with triethylenediamine (TEDA). We used gas phase acid-base reaction to successfully form the ionic frameworks. *In situ* FT-IR analysis, DFT calculations and SXRPD analysis demonstrated that TEDA was selectively deposited on $\mu_3\text{--OH}$ group on Zr-nodes, with stronger adsorption energy than on three other sites ($\mu_3\text{--O}$, $-\text{HCO}_2$, and BTC linker) in MOF-808. It drives the selective decomposition of CK into HOCH and HCl. The selective functionalization of TEDA on MOF-808 created a unique opportunity to achieve the superior removal efficiency of CK (4.05 mmol/g) compared to others (T-Uo-66, T-MIL-100 and 101), especially in humid conditions. We proposed potential structural degradation mechanism from operando IR measurements and DFT calculations in humid circumstance. Results indicated that as the exposure to CK increases, the vibration mode of mono-protonated TEDA on T-MOF-808 and a broad band of $\nu_{\text{s}}(\text{N}^+\text{H})$ associated with the dissociative adsorption of hydrochloric acid increased its intensity. We also confirmed that the diamine functionalized MOF-808 showed excellent removal efficiency for NH₃ and warfare simulant DMMP in humid conditions. Our study can contribute to innovative design of MOFs for efficient removal and sorption of environmental toxic gas and catalysis via selective grafting technology on the molecular level.

CRediT authorship contribution statement

Ga-Young Cha: Methodology, Investigation, Writing - original draft, Validation. **Hoje Chun:** Methodology, Writing - original draft. **Do-Young Hong:** Methodology, Conceptualization, Formal analysis. **Jaegyeom Kim:** Methodology. **Kyung-Ho Cho:** Methodology. **U-Hwang Lee:** Methodology. **Jong-San Chang:** Methodology. **Sam Gon Ryu:** Methodology, Funding acquisition, Formal analysis. **Hae Wan Lee:** Methodology. **Seung-Joo Kim:** Writing - original draft, Methodology. **Byungchan Han:** Writing - original draft, Writing - review & editing, Methodology. **Young Kyu Hwang:** Conceptualization, Writing - original draft, Writing - review & editing, Funding acquisition.

Declaration of Competing Interest

The authors declare that they have no known competing financial interests or personal relationships that could have appeared to influence the work reports in this paper.

Acknowledgements

This work was supported by the Agency for Defense Development of Korea (UE135152 ID and UC190034GD) and partially by the Defense Industry Technology Center (DITC) of Korea (UC5000ID). YKH are kindly grateful to the Institutional Research Program of KRICT (SI-1911-20) for financial support.

Appendix A. Supplementary data

Supplementary material related to this article can be found, in the online version, at doi:<https://doi.org/10.1016/j.jhazmat.2020.122857>.

References

- Barea, E., Montoro, C., Navarro, J.A.R., 2014. Toxic gas removal-metal-organic frameworks for the capture and degradation of toxic gases and vapours. *Chem. Soc. Rev.* 43, 5419–5430.
- Cohen, S.M., 2010. Modifying MOFs: new chemistry. *New Mater. Chem. Sci.* 1, 32–36.
- Couck, S., Denayer, J.F.M., Baron, G.V., Rémy, T., Gascon, J., Kapteijn, F., 2009. An amine-functionalized MIL-53 metal-organic framework with large separation power for CO₂ and CH₄. *J. Am. Chem. Soc.* 131, 6326–6327.

- Cralk, D.J., Levy, G.C., 1982. Carbon-13 and nitrogen-15 nuclear magnetic resonance of polycyclic polyamines. A study of solution N-H hydrogen bonding and protonation. *J. Phys. Chem.* 86, 3893–3900.
- DeCoste, J.B., Peterson, G.W., 2014. Metal-organic frameworks for air purification of toxic chemicals. *Chem. Rev.* 114, 5695–5727.
- DeCoste, J.B., Demasky, T.J., Katz, M.J., Farha, O.K., Hupp, J.T., 2015. A UiO-66 analogue with uncoordinated carboxylic acids for the broad-spectrum removal of toxic chemicals. *New J. Chem.* 39 (39), 2396–2399.
- Farrusseng, D., Aguado, S., Pinei, C., 2009. Metal-organic frameworks: opportunities for catalysis. *Angew. Chem. Int. Ed.* 48, 7502–7513.
- Furukawa, H., Gándara, F., –B. Zhang, Y., Jiang, J., Queen, W.L., Hudson, M.R., Yaghi, O.M., 2014. Water adsorption in porous metal-organic frameworks and related materials. *J. Am. Chem. Soc.* 136, 4369–4381.
- Glover, T.G., Peterson, G.W., Schindler, B.J., Britt, D., Yaghi, O.M., 2011. MOF-74 building unit has a direct impact on toxic gas adsorption. *Chem. Eng. Sci.* 66, 163–170.
- Guzonas, D.A., Irish, D.E., 1988. A raman and infrared spectroscopic study of triethylenediamine (DABCO) and its protonated forms. *Can. J. Chem.* 66, 1249–1257.
- Howarth, A.J., Liu, Y., Li, Z., Wang, T.C., Hupp, J.T., Farha, O.K., 2016. Chemical, thermal and mechanical stabilities of metal-organic frameworks. *Nat. Rev. Mater.* 1, 15018.
- Hwang, Y.K., Hong, D.-Y., Chang, J.-S., Jhung, S.H., Seo, Y.-K., Kim, J., Vimont, A., Daturi, M., Serre, C., Férey, G., 2008. Amine grafting on coordinatively unsaturated metal centers of MOFs: consequences for catalysis and metal encapsulation. *Angew. Chem. Int. Ed.* 120, 4212–4216.
- Katz, M.J., Moon, S.-Y., Mondloch, J.E., Beyzavi, M.H., Stephenson, C.J., Hupp, J.T., Farha, O.K., 2015. Exploiting parameter space in MOFs: a 20-fold enhancement of phosphate-ester hydrolysis with UiO-66-NH₂. *Chem. Sci.* 6, 2286–2291.
- Kaye, S.S., Daily, A., Yaghi, O.M., Long, J.R., 2007. Impact of preparation and handling on the hydrogen storage properties of Zn₄O(1,4-benzenedicarboxylate)₃(MOF-5). *J. Am. Chem. Soc.* 129, 14176–14177.
- Kim, M., Cahill, J.F., Fei, H., Prather, K.A., Cohen, S.M., 2012. Postsynthetic ligand and cation exchange in robust metal-organic frameworks. *J. Am. Chem. Soc.* 134, 18082–18088.
- Kim, C., Cho, H.S., Chang, S., Cho, S.J., Choi, M., 2016. An ethylenediamine-grafted Y zeolite: a highly regenerable carbon dioxide adsorbent via temperature swing adsorption without urea formation. *Energy Environ. Sci.* 9, 1803–1811.
- Kreno, L.E., Leong, K., Farha, O.K., Allendorf, M., Duyne, R.P.V., Hupp, J.T., 2012. Metal-organic framework materials as chemical sensors. *Chem. Rev.* 112, 1105–1125.
- Lee, J., Farha, O.K., Roberts, J., Scheidt, K.A., Nguyen, S.T., Hupp, J.T., 2009. Metal-organic framework materials as catalysts. *Chem. Soc. Rev.* 38, 1450–1459.
- Li, J.-R., Kuppler, R.J., Zhou, H.-C., 2009. Selective gas adsorption and separation in metal-organic frameworks. *Chem. Soc. Rev.* 38, 1477–1504.
- Li, B., Dong, X., Wang, H., Ma, D., Tan, K., Jensen, S., Deibert, B.J., Butler, J., Cure, J., Shi, Z., Thonhauser, T., Chabal, Y.J., Han, Y., Li, J., 2017. Capture of organic iodides from nuclear waste by metal-organic framework-based molecular traps. *Nat. comm.* 8, 1–9.
- Li, J., Huang, H., Liu, P., Song, X., Mei, D., Tang, Y., Wang, X., Zhong, C., 2019. Metal-organic framework encapsulated single-atom Pt catalysts for efficient photocatalytic hydrogen evolution. *J. Catal.* 375, 351–360.
- Liu, G., Chernikova, V., Liu, Y., Zhang, K., Belmabkhout, Y., Shekhar, O., Zhang, C., Yi, S., Eddaoudi, M., Koros, W.J., 2018. Mixed matrix formulations with MOF molecular sieving for key energy-intensive separation. *Nat. Mater.* 17, 283–289.
- Mahle, J.J., Peterson, G.W., Schindler, B.J., Smith, P.B., Rossin, J.A., Wagner, G.W., 2010. Role of TEDA as an activated carbon impregnant for the removal of cyanogen chloride from air streams: synergistic effect with Cu(II). *J. Phys. Chem. C* 114, 20083–20090.
- Mizrahi, D.M., Saphier, S., Columbus, I., 2010. Efficient heterogeneous and environmentally friendly degradation of nerve agents on a tungsten-based POM. *J. Hazard. Mater.* 179, 495–499.
- Moon, S.-Y., Liu, Y., Hupp, J.T., Farha, O.K., 2015. Instantaneous hydrolysis of nerve agent simulants with a six-connected zirconium-based metal-organic framework. *Angew. Chem. Int. Ed.* 54, 6795–6799.
- Munro, N.B., Talmage, S.S., Griffin, G.D., Waters, L.C., Watson, A.P., King, J.F., Hauschild, V., 1999. The sources, fate, and toxicity of chemical warfare agent degradation products. *Environ. Health Perspect.* 107, 933–974.
- Padial, N.M., Procopio, E.Q., Montoro, C., López, E., Oltra, J.E., Colombo, V., Maspero, A., Masciocchi, N., Galli, S., Senkovska, I., Kaskel, S., Barela, E., Navarro, J.A.R., 2013. Highly hydrophobic isoreticular porous metal-organic frameworks for the capture of harmful volatile organic compounds. *Angew. Chem. Int. Ed.* 52, 8290–8294.
- Peng, Y., Huang, H., Liu, D., Zhong, C., 2016. Radioactive barium ion trap based on metal-organic framework for efficient and irreversible removal of barium from nuclear wastewater. *ACS Appl. Mater. Interfaces* 8, 8527–8535.
- Peng, Y., Huang, H., Zhang, Y., Kang, C., Chen, S., Song, L., Liu, D., Zhong, C., 2018. A versatile MOF-based trap for heavy metal ion capture and dispersion. *Nat. Commun.* 9, 187–195.
- Peterson, G.W., Wagner, G.W., Keller, J.H., Rossin, J.A., 2010. Enhanced cyanogen chloride removal by the reactive zirconium hydroxide substrate. *Ind. Eng. Chem. Res.* 49, 11182–11187.
- Peterson, G.W., Rossin, J.A., DeCoste, J.B., Killops, K.L., Browne, M., Valdes, E., Jones, P., 2013. Zirconium hydroxide-metal-organic framework composites for toxic chemical removal. *Ind. Eng. Chem. Res.* 52, 5462–5469.
- Pirc, G., Mavri, J., Novič, M., Stare, J., 2012. Virtually nonexistent correlation between the OH stretching frequency and the instantaneous geometry in the short hydrogen bond of sodium hydrogen bis(sulfate): advanced chemometrics analysis. *J. Phys. Chem. B* 116, 7221–7231.
- Platero-Prats, A.E., League, A.B., Bernales, V., Ye, J., Gallington, L.C., Vjunov, A., Schweitzer, N.M., Li, Z., Zheng, J., Mehdi, B.L., Stevens, A.J., Dohnalkova, A., Balasubramanian, M., Farha, O.K., Hupp, J.T., Browning, N.D., Fulton, J.L., Camaioni, D.M., Lercher, J.A., Truhlar, D.G., Gagliardi, L., Cramer, C.J., Chapman, K.W., 2017. Bridging zirconia modes within a metal-organic framework via catalytic Ni-hydroxo clusters to form heterobimetallic nanowires. *J. Am. Chem. Soc.* 139, 10410–10418.
- Purohit, A.K., Kumar, A., Singh, V., Goud, D.R., Jain, R., Dubey, D.K., 2014. Polymer-supported sulfonated magnetic resin: an efficient reagent for esterification of O-alkyl alkylphosphonic and carboxylic acids. *Tetrahedron Lett.* 55, 6844–6846.
- Rosi, N.L., Eckert, J., Eddaoudi, M., Vodak, D.T., Kim, J., O'Keeffe, M., Yaghi, O.M., 2003. Hydrogen storage in microporous metal-organic frameworks. *Science* 16, 1127–1129.
- Shearer, G.C., Forsey, S., Chavan, S., Bordiga, S., Mathisen, K., Bjørgen, M., Svelde, S., Lillerud, K.P., 2013. In situ infrared spectroscopic and gravimetric characterization of the solvent removal and dehydroxylation of the metal organic frameworks UiO-66 and UiO-67. *Top. Catal.* 56, 770–782.
- Valerkar, A.H., Cho, K.-H., Chitale, S.K., Hong, D.-Y., Cha, G.-Y., Lee, U.-H., Hwang, D.W., Serre, C., Chang, J.-S., Hwang, Y.K., 2016. Catalytic transfer hydrogenation of ethyl levulinic to γ -valerolactone over zirconium-based metal-organic frameworks. *Green Chem.* 18, 4542–4552.
- Wang, G., Sharp, C., Plonka, A.M., Wang, Q., Frenkel, A.I., Guo, G., Smith, C., Kollar, J., Troya, D., Morris, J.R., 2017. Mechanism and kinetics for reaction of the chemical warfare agent simulant DMMP(g) with zirconium(IV) MOFs: an ultrahigh-vacuum and DFT study. *J. Phys. Chem. C* 21, 11261–11272.
- Xie, L.-H., Liu, X.-M., He, T., Li, J.-R., 2018. Metal-organic frameworks for the capture of trace aromatic volatile organic compounds. *Chem. Eng. J.* 191, 1911–1927.
- Yaghi, O.M., O'Keeffe, M., Ockwing, N.W., Chae, H.K., Eddaoudi, M., Kim, J., 2003. Reticular synthesis and the design of new materials. *Nature* 423, 705–714.
- Yang, Q., Wiersum, A.D., Llewellyn, P.L., Guillerm, V., Serre, C., Maurin, G., 2011. Functionalizing porous zirconium tetraphthalate UiO-66(Zr) for natural gas upgrading: a computational exploration. *Chem. Commun.* 47, 9603–9605.
- Yang, D., Bernales, V., Islamoglu, T., Farha, O.K., Hupp, J.T., Cramer, C.J., Gagliardi, L., Gates, B.C., 2016. Tuning the surface chemistry of metal organic framework nodes: proton topology of the metal-oxide-like Zr₆ nodes of UiO-66 and Nu-1000. *J. Am. Chem. Soc.* 138, 15189–15196.
- Yang, D., Ortúñoz, M.A., Bernales, V., Cramer, C.J., Gagliardi, L., Gates, B.C., 2018. Structure and dynamics of Zr608 metal-organic framework node surfaces probed with ethanol dehydration as a catalytic test reaction. *J. Am. Chem. Soc.* 140, 3751–3759.
- Yoon, J.W., Chang, H., Lee, S.-J., Hwang, Y.K., Hong, D.-Y., Lee, S.-K., Lee, J.S., Jang, S., Yoon, T.-U., Kwac, K., Jung, Y., Pillai, R.S., Faucher, F., Vimont, A., Daturi, M., Férey, G., Serre, C., Maurin, G., Bae, Y.-S., Chang, J.-S., 2017. Selective nitrogen capture by porous hybrid materials containing accessible transition metal sites. *Nat. Mater.* 16, 526–531.
- Yuan, S., Chen, Y.-P., Qin, J., Lu, W., Wang, X., Zhang, Q., Bosch, M., Liu, T.-F., Lian, X., Zhou, H.-C., 2015. Cooperative cluster metalation and ligand migration in zirconium metal-organic frameworks. *Angew. Chem. Int. Ed.* 54, 14696–14700.
- Yuan, S., Feng, L., Wang, K., Pang, J., Bosch, M., Lollar, C., Sun, Y., Qin, J., Yang, X., Zhang, P., Wang, Q., Zou, L., Zhang, Y., Zhang, L., Fang, Y., Li, J., Zhou, H.-C., 2018. Stable metal-organic frameworks: design, synthesis, and applications. *Adv. Mater.* 30, 1704303.
- Zhang, Y., Zhang, X., Lyu, J., Otake, K., Wang, X., Redfern, L.R., Malliakas, C.D., Li, Z., Islamoglu, T., Wang, B., Farha, O.K., 2018. A flexible metal-organic framework with 4-connected Zr₆ nodes. *J. Am. Chem. Soc.* 140, 11179–11183.